APL Materials

Tunable Curie temperature in layered ferromagnetic $Cr_{5+x}Te_8$ single crystals

Cite as: APL Mater. **8**, 031101 (2020); https://doi.org/10.1063/1.5143387
Submitted: 23 December 2019 . Accepted: 13 February 2020 . Published Online: 02 March 2020

Luo-Zhao Zhang, Xiu-De He, An-Lei Zhang, Qi-Ling Xiao, Wen-Lai Lu, Fei Chen, Zhenjie Feng, Shixun Cao, Jincang Zhang, and Jun-Yi Ge

Tunable Curie temperature in layered ferromagnetic $Cr_{5+x}Te_8$ single crystals

Cite as: APL Mater. 8, 031101 (2020); doi: 10.1063/1.5143387
Submitted: 23 December 2019 • Accepted: 13 February 2020 •
Published Online: 2 March 2020

Luo-Zhao Zhang,[1] Xiu-De He,[1] An-Lei Zhang,[1] Qi-Ling Xiao,[1] Wen-Lai Lu,[1] Fei Chen,[1] Zhenjie Feng,[1] Shixun Cao,[1,2] Jincang Zhang,[1] and Jun-Yi Ge[1,3,a)]

AFFILIATIONS

[1]Materials Genome Institute, Shanghai University, 200444 Shanghai, China
[2]Department of Physics, Shanghai University, 200444 Shanghai, China
[3]Shanghai Key Laboratory for High Temperature Superconductors, Shanghai University, 200444 Shanghai, China

[a)]**Author to whom correspondence should be addressed:** junyi_ge@t.shu.edu.cn

ABSTRACT

The relatively low Curie temperature (T_c) in recently discovered two-dimensional ferromagnetic (FM) materials has limited their potential applications in designing next generation electronics. Searching for new low-dimensional layered materials with room-temperature T_c is highly needed. Here, we report the study of layered FM materials $Cr_{5+x}Te_8$ ($x = -0.10, 0.11, 0.56, 1$) in which T_c can be well manipulated by the Cr content. Single crystalline $Cr_{5+x}Te_8$ samples have been synthesized and characterized by energy dispersive x-ray spectroscopy, x-ray diffraction, and magnetization measurements. We have found that T_c increases monotonically with Cr content and reaches 313 K at $x = 1$. While the FM coupling is enhanced with an increase in the Cr content, the antiferromagnetic (AFM) phase at low temperatures is suppressed. Due to the competition of FM and AFM phases, a wasp-waist loop is observed on isothermal magnetization curves. A magnetic flip occurs by changing the temperature and magnetic field to overcome the flipping energy barrier. Our results indicate that the $Cr_{5+x}Te_8$ system serves as a promising platform to tune the 2D ferromagnetism in layered materials.

I. INTRODUCTION

The exotic electronic properties and tremendous applications of graphene[1] have ignited the research boom into van der Waals (vdWs) force connected, two-dimensional (2D) materials. Among all the 2D materials, the recently discovered 2D magnetic materials have been at the focus of scientific community due to the breakthrough of fundamental theory and the practical applications in designing new generation electronic devices.[2–4] The main research objects include CrI_3,[5–7] $Cr_2Ge_2Te_6$,[8,9] $Cr_2Si_2Te_6$,[10] and Fe_3GeTe_2.[11] For all the materials mentioned above, the magnetic properties have been studied extensively in various forms from monolayer to bulk. However, most reported 2D ferromagnetic (FM) materials show a notable limit that the Curie temperature is much below room temperature, e.g., 61 K for CrI_3, 61 K for $Cr_2Ge_2Te_6$, and 32 K for $Cr_2Si_2Te_6$. Many approaches have been applied to manipulate their magnetic properties, for example, by using liquid/solid ion gating[11–13] or simply electrostatic doping.[5,6] One typical success is that, by using a liquid ion gate, the Curie temperature of a few layer Fe_3GeTe_2 can be tuned up to 300 K.[11] Looking for new layered ferromagnetic materials with intrinsic room-temperature, T_c is extremely needed.

Recent theoretical calculations suggest that the layered Cr_xTe_y compounds may be good candidates for RT 2D FM materials.[14,15] Many different forms of Cr_xTe_y have been synthesized including CrTe,[16] Cr_2Te_3,[17,18] Cr_3Te_4,[19] and Cr_5Te_8.[20,21] In these compounds, there are alternating stacks of Cr-deficient and Cr-full layers along the c-axis.[22,23] Cr content has been found to play a vital role in determining the structure and magnetic properties. Among all CrTe compounds, Cr_5Te_8 compounds with T_c ranging between 180 K and 240 K have been studied extensively.[23] It is reported that Cr_5Te_8 crystallize in monoclinic or trigonal structures, similar to the NiAs-type structure.[24,25] With an increase in the temperature, the lattice constants a and b decrease while c

increases, leading to a slight increase in the cell volume.[26] The magnetic structures have also been studied through neutron diffraction measurements.[18,27] The electronic band structure calculations performed on CrTe, Cr_2Te_3, and Cr_3Te_4 suggest that Cr $3d_{z^2}$-Cr $3d_{z^2}$ along the crystallographic c-direction overlap strongly with Cr $3d_{z^2}$-Cr $3d_{z^2}$ orbital at a relatively smaller nearest neighbor Cr–Cr distance.[22] Recent reports for critical behavior research of Cr_5Te_8 confirmed that short range type interaction of weak itinerant ferromagnetism persists in bulk with remarkable magnetocrystalline anisotropy.[28] Besides, magnetocaloric effects of Cr_5Te_8 were reported in several studies, suggesting that the ferromagnetic interaction of Cr_5Te_8 is close to the boundary of a short-range type and long-range type order.[29,30] Anomalous Hall effect (AHE) and topological Hall effect were observed in $Cr_{4.14}Te_8$ and Cr_5Te_8.[20,21,31] With all the exotic properties discovered, it is necessary to systematically investigate the evolution of magnetic properties in the $Cr_{5+x}Te_8$ system.

Here, by using the chemical vapor transport method, we synthesize high quality $Cr_{5+x}Te_8$ single crystals with x ranging between −0.11 and 1. We have found that, with an increase in the Cr content, T_c increases monotonically from 200 K to 313 K. Their magnetic properties are studied systematically. Pronounced anisotropic magnetic properties have been found in all crystals. Meanwhile, the competition between ferromagnetic and antiferromagnetic (AFM) phases leads to a spin-glass like behavior at relatively low magnetic fields. Moreover, spin-flip and wasp-waist loops were discovered in $Cr_{5.11}Te_8$, which may be attributed to the coexistence of AFM and FM phases. Although T_c is enhanced drastically with Cr content, all samples show soft ferromagnetism with small coercivity.

II. EXPERIMENTAL

Single crystalline samples with the composition of $Cr_{5+x}Te_8$ were grown by the chemical vapor transport method.[32] Cr (99.99%, Alfa Aesar) and Te powders (99.99%, Alfa Aesar) were thoroughly mixed and then sealed into a quartz tube with a partial pressure of argon. The iodine was used as a transport agent. The quartz tubes were heated to 400 °C in 4 h and kept at the temperature for 10 h before further heating up to 1000 °C on one side, while at the same time, the other side was heated to 820 °C. Single crystals with layered structures and metallic luster were observed at the cold side of the tube. The compositions of all single crystals were characterized by the energy dispersive x-ray (EDX) spectroscopy. Single crystal compositions described in this paper all refer to the EDX values. The single crystal x-ray diffraction patterns were collected at room temperature with Cu K_α. The data of magnetization were measured by using a quantum design Physical Property Measurement System (PPMS-14T) with a vibrating sample magnetometer option.

III. RESULTS AND DISCUSSIONS

Figure 1(a) shows one optical image of one single crystal with $x = -0.1$. The bottom left image presents the large view of the crystal with layered structures. The bottom right image is element

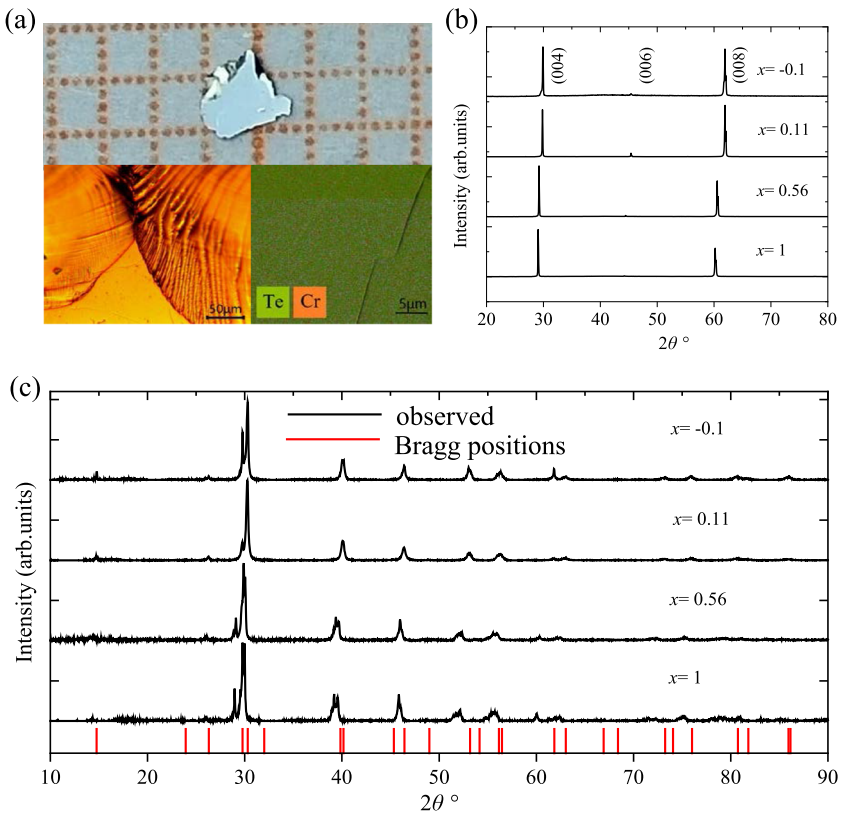

FIG. 1. (a) The optical image of one typical as-grown crystal $Cr_{4.9}Te_8$. The bottom left image shows the layer structure of the crystal. The bottom right image shows the element distribution in the single crystal, with the green and orange bars representing the Te and Cr elements, respectively. (b) The x-ray diffraction patterns of single crystalline $Cr_{5+x}Te_8$ showing (00L) diffraction peaks. (c) Powder XRD patterns of four $Cr_{5+x}Te_8$ crystals, the black curves show the experiment data, and the vertical red straight lines represent the standard Bragg reflections of Cr_5Te_8 with the space group of $p\bar{3}m1$.

distribution of single crystal taken by the scanning electron microscope with an EDX. Cr and Te elements are represented by green and orange bars, respectively. It is seen that both elements were homogeneously distributed in the sample. The crystal structure was also checked by using the XRD. Figure 1(b) presents the XRD patterns of four single crystals with $x = -0.1$, 0.11, 0.56, and 1. For all the crystals, only the (00L) Bragg peaks are observed, suggesting that c-axis is perpendicular to the crystal surface.[28,29] We did not observe any extra peak within the resolution limit of our XRD instrument. This indicates the good crystallinity of our crystal. As shown in Fig. 1(c), the powder XRD patterns of $Cr_{4.9}Te_8$ and $Cr_{5.11}Te_8$ fit well with the $p\bar{3}m1$ space group. By increasing the Cr content, the diffraction peaks slightly move to lower θ values, and no other extra peak appears, indicating that more Cr contents only increase the lattice parameter but do not change the crystal structure. Therefore, we conclude all $Cr_{5+x}Te_8$ samples crystallized in trigonal structure with space group $p\bar{3}m1$.

To explore the magnetic properties, temperature dependence of magnetization measurements along both the ab-plane and the c-axis has been performed for all the samples under various magnetic fields and in a large temperature range. Figures 2(a) and 2(b) present the results for $x = 0.56$ sample measured through both zero-field-cooling (ZFC) and field-cooling (FC) processes with $H \| c$. A paramagnetic to ferromagnetic phase transition is clearly observed. At low temperatures, the magnetization observed in ZFC mode tends to deviate from that of the FC curve. Such a discrepancy can be attributed to the appearance of a canted AFM (c-AFM) structure with a small AFM component along the ab-plane and a large ferromagnetic component along the c-axis.[26] We can define $T_{c\text{-}AFM}$ as the temperature where ZFC and FC curves start to separate. It is seen from Fig. 2(e) that, with an increase in the magnetic field, $T_{c\text{-}AFM}$ was progressively suppressed (e.g., $H = 5000$ Oe). Similar results have also been observed in other samples with different extra Cr contents.

Figures 2(c) and 2(d) show the temperature dependencies of the magnetization measured in the field-cooled (FC) process at a magnetic field of $H = 3000$ Oe for both directions. The magnetization increases clearly with an increase in the Cr content. The inset of Fig. 2(f) shows the $1/\chi$ vs T plot for $x = 1$, from which we can extract the Curie temperature (T_c) by fitting the data at a high temperature regime. The observed T_c values for both field directions are plotted in Fig. 2(f). A slight difference in T_c is observed for both directions.

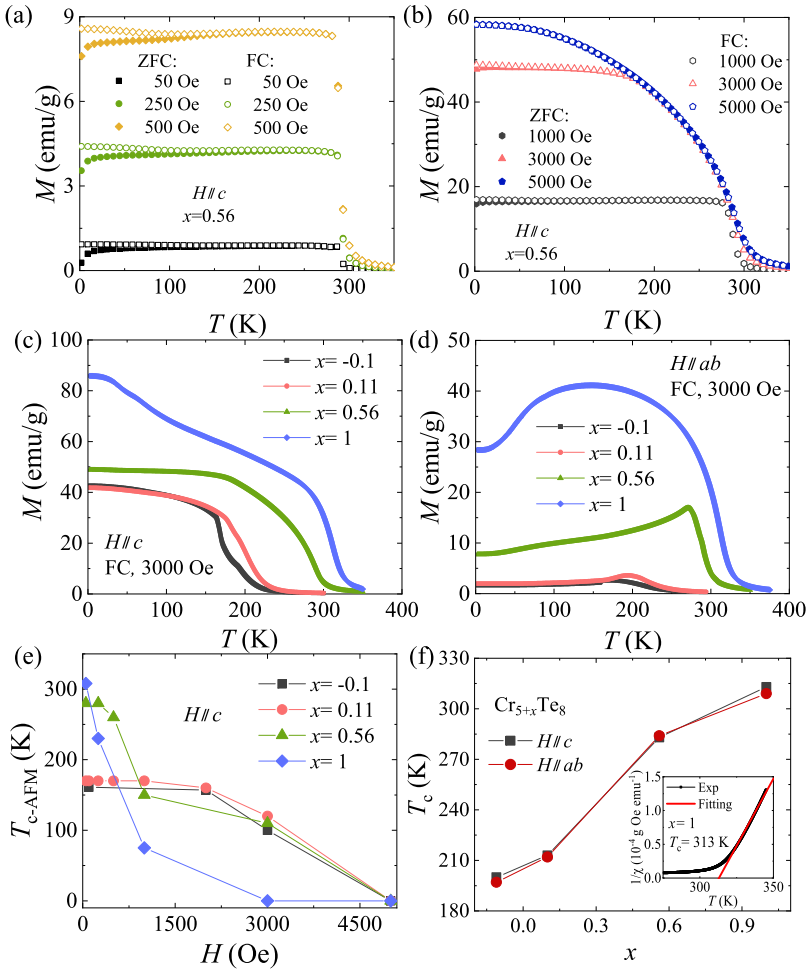

FIG. 2. [(a) and (b)] Temperature dependence of magnetization M-T for $x = 0.56$ with $H \| c$ at applying fields between 50 Oe and 5000 Oe. [(c) and (d)] Temperature dependence of the magnetization M measured with $H = 3000$ Oe with the field applied parallel to the c-axis and the ab-plane, respectively. (e) Field dependence of the separating temperature $T_{c\text{-}AFM}$, indicating the appearance of canted antiferromagnetism. (f) Curie temperature as a function of Cr content. The inset shows how T_c is defined by fitting the data with the Curie–Weiss law.

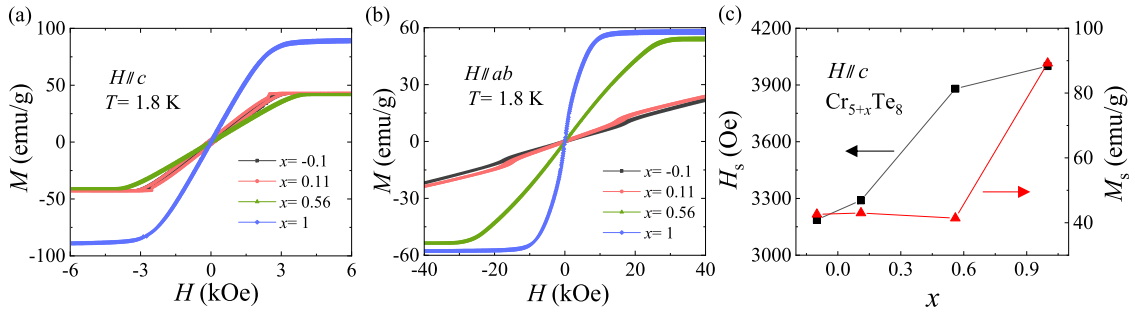

FIG. 3. Isothermal magnetization loops of $Cr_{5+x}Te_8$ measured at T = 1.8 K for (a) $H \| c$ and (b) $H \| ab$. (c) The saturation magnetization (M_s) and the saturation magnetic fields (H_s) derived from M-H curves with $H \| c$.

The ferromagnetic phase transition temperature T_c of the $Cr_{5+x}Te_8$ samples increases dramatically from 200 K with $x = -0.1$ K to 313 K with $x = 1$. The results suggest that the extra Cr atoms intercalate into $CrTe_2$ layers. The local spins of intercalated Cr ions align ferromagnetically through Te 5*d*; this indirect exchange interaction enhances the Curie temperature. Besides the dramatic increase in T_c, all M-T curves show rather complex magnetic phases and anisotropy. For example, the magnetization saturates at low temperatures when the field is along the *c*-axis, while for $H \| ab$, the magnetization slowly decreases below T_c.

To further explore the magnetic state at low temperatures, we have performed the isothermal magnetization measurements with $H \| c$ and $H \| ab$. Figures 3(a) and 3(b) show the results observed at T = 1.8 K. For applied magnetic field along the *c*-axis, the saturated magnetization (around 3000 Oe) manifests ferromagnetic ground states for all the samples. When applying a magnetic field along the *ab*-plane, no magnetization saturation is observed for samples with relatively low extra Cr content ($x = -0.1$, 0.11) even at much higher magnetic field (H = 4 T) as reported before.[30,33] This can be explained by the existence of canted AFM in the *ab*-plane at low temperature. The coexistence between canted AFM and FM leads to the unsaturated magnetization. Another evidence for the coexistence of AFM and FM is the observation of wasp-waist magnetization loops for sample of x = 0.11. Similar behaviors have been predicted in Ref. 34. For $x = 0.56$ and $x = 1$, magnetization saturation is observed, however, at magnetic fields (29 kOe and 13 kOe) much higher than that with $H \| c$. This can be attributed to the large amount of extra Cr atoms, which give rise to a strong FM coupling in the *ab*-plane. All data suggest that the *c*-axis is the easy magnetization axis, along which the orbital covalence of Cr 3*d*-Te 5*P* and their strong overlapping result in a shorter distance between Cr atoms than that in the *ab*-plane.[22] Along the *c*-axis, there is no obvious difference in saturated magnetization value for samples with $x = -0.1$, 0.11, and 0.56. Along the *ab*-plane, the saturated magnetization for $x = 0.56$ and $x = 1$ samples show a slight difference. This may suggest that there exists a critical value of extra Cr content. Only above such a value, the magnetic ground state can be dramatically changed.

In order to further clarify the competition and coexistence of AFM and FM states mentioned above, a single crystal with $x = 0.11$ is chosen for careful magnetization measurements. At low temperature, ZFC and FC curves show significant split [Fig. 4(a)], similar to that of x = 0.56 [Figs. 2(a) and 2(b)]. This can be ascribed to the appearance of canted AFM magnetic structure along the *ab*-plane with a large ferromagnetic component along the *c*-axis at low temperature. The magnetic structure has already been confirmed by the neutron diffraction experiment.[26] With an increase in the magnetic field, the canted AFM is slowly suppressed above H = 5000 Oe [Fig. 4(b)]. The wasp-waist loop appears at T = 2 K with $H \| ab$, as shown in the inset of Fig. 4(c). A small magnetization jump appears in the direction of $H \| c$ at T = 2 K [Fig. 4(d)]. From the magnetization loops in Figs. 4(c) and 4(d), it is also clear that, at low temperatures, the coexistence of canted AFM and FM results in the wasp-waist loop. At high temperatures, paramagnetic behaviors are observed, while at intermediate temperatures below T_c, ferromagnetism dominates.

When increasing the Cr content ($x = 0.56$, $x = 1$), the wasp-waist loops disappear and the magnetization becomes easily saturated. This means that sufficient Cr atoms enhance FM coupling; meanwhile, the AFM phase decreases. As shown in the inset of Fig. 4(d), a small jump can be observed, which is characteristic of the spin-flip behavior, the small jumps also appear in another layered ferromagnet Fe_3GeTe_2,[35] considering there is a competing antiferromagnetism in itinerant ferromagnetism Fe_3GeTe_2.[36] We speculate that the small jumps may result from the transformation of a fraction of the FM phase into the AFM phase when the magnetic field decreases from saturation field values.

For sample containing the minimum Cr content ($x = -0.1$), as shown in Figs. 5(a) and 5(b), a new phenomenon can be derived from the ZFC, FC, and FCW magnetization curves. For both ZFC and FC curves with field along the *c*-axis, at the temperature of 159 K, the magnetization drops almost vertically, while for M-T curves with the $H \| ab$-plane, an abrupt increase in magnetization is observed at the same temperature. This may indicate a magnetic moment flipping from the *c*-direction to the *ab*-plane at 159 K. However, the absolute value of magnetization change is much smaller for the $H \| ab$-plane. We may speculate that there exist magnetic domains with the magnetic moment pinned along the *c*-axis. At low temperatures, the energy is not enough to move the pinned domains. With an increase in the temperature to a high enough value, thermal fluctuations gradually weaken the pinning force and finally depin the domains, which leads to the disordered arrangement of the magnetic moment, so the magnetization along the *c*-axis decreases. This depinning process does not require a high magnetic field. Therefore, when the applied field is along the *ab*-plane, the disordered magnetic

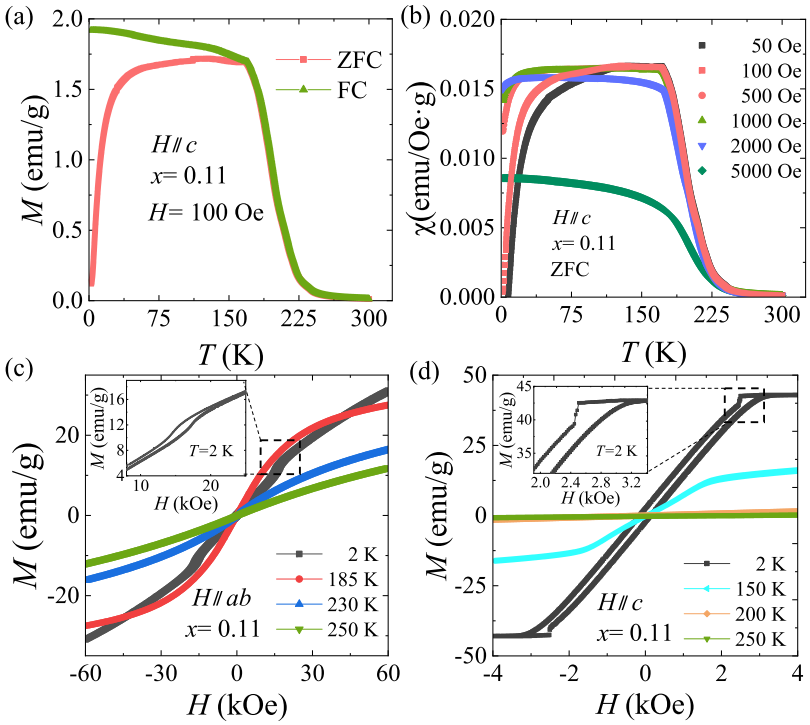

FIG. 4. (a) Temperature dependence of magnetization (*M*-*T*) measured through ZFC and FC processes for x = 0.11 under a magnetic field H = 100 Oe along *c*-axis. (b) ZFC *M*-*T* curves for sample x = 0.11 measured under different magnetic field with $H \| c$. (c) Isothermal magnetization loops of x = 0.11 measured at different temperatures with $H \| ab$. The inset shows the enlarged view of the indicated *M*-*H* loop at T = 2 K. (d) *M*-*H* loops measured with $H \| c$ at different temperatures. The inset shows the close-up of the curve at T = 2 K marked by gray dashed–dotted line rectangle.

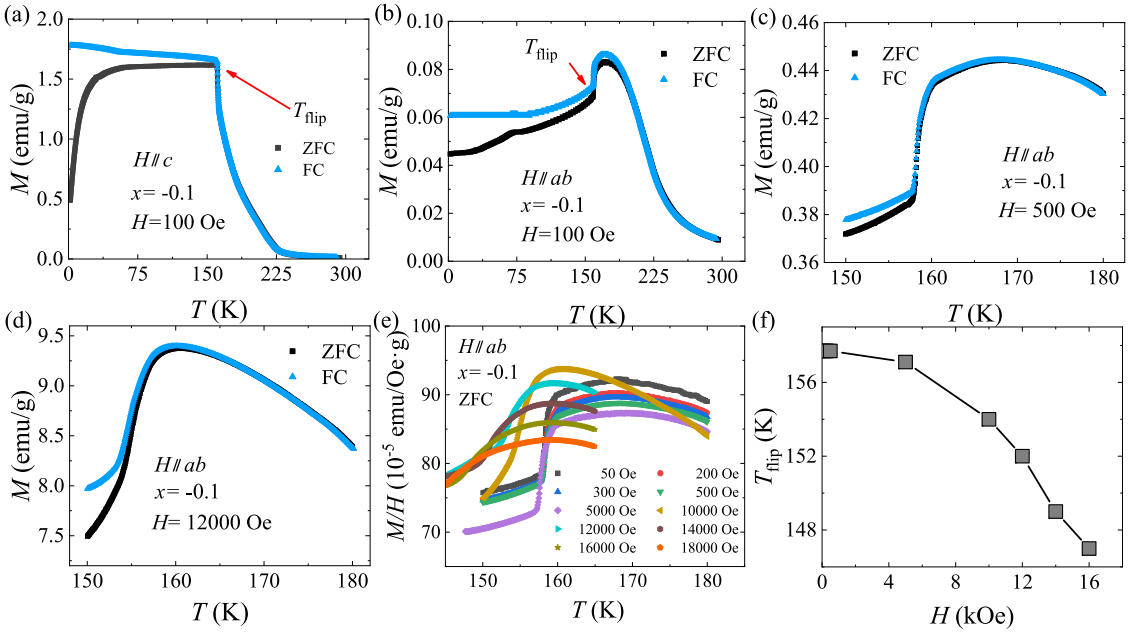

FIG. 5. Temperature dependence of magnetization measured under ZFC and FC modes for the sample of x = −0.1 at 100 Oe with (a) $H \| c$ and (b) $H \| ab$. In both (a) and (b), the spin flip points are marked by the red arrows. *M*-*T* curves measured at magnetic field (c) H = 500 Oe and (d) H = 12 kOe in the direction of $H \| ab$. (e) ZFC susceptibility curves measured under different magnetic fields with $H \| ab$. The spin flipping is progressively suppressed to lower temperatures. (f)The derived spin-flip temperature T_{flip} as a function of applied magnetic field.

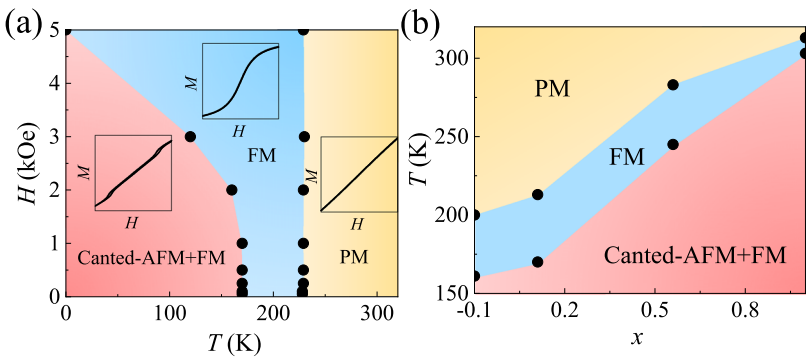

FIG. 6. (a) Typical magnetic phase diagram for $Cr_{5+x}Te_8$ with $x = 0.11$ and the magnetic field parallel to the *ab*-plane. Three magnetic phases can be observed. The insets show the typical magnetization loops for each magnetic phase. (b) Magnetic phase diagram of $Cr_{5+x}Te_8$ ($x = -0.1$, 0.11, 0.56, 1) with applied field $H = 100$ Oe in the *ab*-plane (the *c*-axis shows no differences).

moments rearrange in the *ab*-plane, and magnetization increases. Here, we define the spin flipping temperature T_{flip} as the temperature where a noticeable change can be seen on the M-T curves [as shown by the red arrows in Figs. 5(a) and 5(b)]. We have found that, at large magnetic fields, T_{flip} moves to lower temperature [Figs. 5(c)–5(e)]. The relation of T_{flip} vs (H) is summarized in Fig. 5(f), where a monotonic decrease in T_{flip} is observed. Moreover, the magnetization change at T_{flip} becomes less obvious. This suggests that there exists a flipping energy barrier at relatively small magnetic fields and below T_{flip}. Only at high enough temperature and magnetic fields, the system can have enough energy to overcome the barrier and magnetization flipping occurs. More approaches are need to further clarify such a phenomenon, e.g., by using ac magnetization measurements to probe the possible glassy behavior around T_{flip}.

The data for $x = 0.11$ are summarized in a magnetic phase diagram, where three phases are clearly seen: (1) a coexistence phase with ferromagnetism and canted antiferromagnetism (canted-AFM + FM), (2) ferromagnetic phase (FM), and (3) paramagnetic phase (PM). The characteristic magnetization loop for each magnetic phase is also indicated as the inset. From the phase diagram, we can clearly see the competition between the FM and canted-AFM phase when changing the magnetic field. With an increase in the magnetic field, the FM phase is enhanced, while the canted-AFM + FM phase is suppressed. The PM phase is not affected in our applied field regime. Figure 6(b) shows the T–x phase diagram for $Cr_{5+x}Te_8$ ($x = -0.1$, 0.11, 0.56, 1) with applied field $H = 100$ Oe. With an increase in the Cr content, the FM phase is enhanced to the room temperature regime and becomes narrower. The canted-AFM phase appears at higher temperature more close to T_c. Further experimental work is needed to clarify, at even higher Cr contents, whether the pure FM phase disappears or not.

IV. CONCLUSIONS

In summary, a series of layered ferromagnetic $Cr_{5+x}Te_8$ ($x = -0.1$ to 1) single crystals have been grown by chemical vapor transport methods. By increasing the Cr content, T_c can be tuned monotonically from 200 K to 313 K. Ferromagnetism has been found to coexist with canted ferromagnetism in the system, leading to the observation of wasp-waist magnetization loops and magnetization flipping. All the results have shown that the Cr–Te system provides a suitable platform to study low dimensional ferromagnetism at a room temperature regime.

ACKNOWLEDGMENTS

This study was supported by the National Key Research and Development Program of China (Grant No. 2018YFA0704300) and the National Natural Science Foundation of China (Grant No. 11804217). J.-Y.G. thanks the support by the Program for Professor of Special Appointment (Eastern Scholar) at Shanghai Institutions of Higher Learning.

REFERENCES

[1] A. K. Geim, Science **324**, 1530 (2009).
[2] D. Zhong, K. L. Seyler, X. Yu, L. Peng, R. Cheng, N. Sivadas, B. Huang, E. Schmidgall, T. Taniguchi, K. Watanabe, M. A. McGuire, W. Yao, D. Xiao, K. M. C. Fu, and X. D. Xu, Sci. Adv. **3**, e1603113 (2017).
[3] A. K. Geim and I. V. Grigorieva, Nature **499**, 419 (2013).
[4] J. T. Heron, M. Trassin, K. Ashraf, M. Gajek, Q. He, S. Y. Yang, D. E. Nikonov, Y.-H. Chu, S. Salahuddin, and R. Ramesh, Phys. Rev. Lett. **107**, 217202 (2011).
[5] S. W. Jiang, L. Z. Li, Z. F. Wang, K. F. Mak, and J. Shan, Nat. Nanotechnol. **13**, 549 (2018).
[6] S. W. Jiang, J. Shan, and K. F. Mak, Nat. Mater. **17**, 406 (2018).
[7] B. Huang, G. Clark, D. R. Klein, D. MacNeill, E. Navarro-Moratalla, K. L. Seyler, N. Wilson, M. A. McGuire, D. H. Cobden, D. Xiao, W. Yao, P. Jarillo-Herrero, and X. Xu, Nat. Nanotechnol. **13**, 544 (2018).
[8] Y. Liu and C. Petrovic, Phys. Rev. B **96**, 054406 (2017).
[9] G. T. Lin, H. L. Zhuang, X. Luo, B. J. Liu, F. C. Chen, J. Yan, Y. Sun, J. Zhou, W. J. Lu, P. Tong, Z. G. Sheng, Z. Qu, W. H. Song, X. B. Zhu, and Y. P. Sun, Phys. Rev. B **95**, 245212 (2017).
[10] T. J. Williams, A. A. Aczel, M. D. Lumsden, S. E. Nagler, M. B. Stone, J.-Q. Yan, and D. Mandrus, Phys. Rev. B **92**, 144404 (2015).
[11] Y. J. Deng, Y. J. Yu, Y. C. Song, J. Z. Zhang, N. Z. Wang, Z. Y. Sun, Y. F. Yi, Y. Z. Wu, S. W. Wu, J. Y. Zhu, J. Wang, X. H. Chen, and Y. B. Zhang, Nature **563**, 94 (2018).
[12] F. Matsukura, Y. Tokura, and H. Ohno, Nat. Nanotechnol. **10**, 209 (2015).
[13] M. Weisheit, S. Fähler, A. Marty, Y. Souche, C. Poinsignon, and D. Givord, Science **315**, 349 (2007).
[14] X. W. Zhang, B. Wang, Y. L. Guo, Y. H. Zhang, Y. F. Chen, and Z. L. Wang, Nanoscale Horiz. **4**, 859 (2019).
[15] Y. Zhu, X. H. Kong, T. D. Rhone, and H. Guo, Phys. Rev. Mater. **2**, 081001 (2018).
[16] T. Eto, M. Ishizuka, S. Endo, T. Kanomata, and T. Kikegawa, J. Alloys Compd. **315**, 16 (2001).

[17]F. Wang, J. Du, F. Sun, R. F. Sabirianov, N. Al-Aqtash, D. Sengupta, H. Zeng, and X. H. Xu, Nanoscale **10**, 11028 (2018).
[18]T. Hamasaki, T. Hashimoto, Y. Yamaguchi, and H. Watanabe, Solid State Commun. **16**, 895 (1975).
[19]B. Hessen, T. Siegrist, T. Palstra, S. M. Tanzler, and M. L. Steigerwald, Inorg. Chem. **32**, 5165 (1993).
[20]Y. H. Wang, J. Yan, J. B. Li, S. S. Wang, M. Song, J. P. Song, Z. H. Li, K. Chen, Y. L. Qin, L. S. Ling, H. F. Du, L. Cao, X. Luo, Y. M. Xiong, and Y. P. Sun, Phys. Rev. B **100**, 024434 (2019).
[21]Y. Liu and C. Petrovic, Phys. Rev. B **98**, 195122 (2018).
[22]J. Dijkstra, H. H. Weitgering, C. F. van Bruggen, C. Haas, and R. A. de Groot, J. Phys.: Condens. Matter **1**, 9141 (1989).
[23]H. Ipser, K. L. Komarek, and K. O. Klepp, J. Less-Common Met. **92**, 265 (1983).
[24]M. Akram and F. M. Nazar, J. Mater. Sci. **2**, 441 (1983).
[25]K. Lukoschus, S. Kraschinski, C. Nather, W. Bensch, and R. K. Kremer, J. Solid State Chem. **177**, 951 (2004).
[26]Z. L. Huang, W. Kockelmann, M. Telling, and W. Bensch, Solid State Sci. **10**, 1099 (2008).
[27]A. F. Andresen, Acta Chem. Scand. **24**, 3495 (1970).
[28]Y. Liu and C. Petrovic, Phys. Rev. B **96**, 134410 (2017).
[29]X. Zhang, T. L. Yu, Q. Y. Xue, M. Lei, and R. Z. Jiao, J. Alloys Compd. **750**, 798 (2018).
[30]R. Mondal, R. Kulkarni, and A. Thamizhavel, J. Magn. Magn. Mater. **483**, 27 (2019).
[31]Y. Yan, X. Luo, G. T. Lin, F. C. Chen, J. J. Gao, Y. Sun, L. Hu, P. Tong, W. H. Song, S. Z. Gao, W. J. Lu, X. B. Zhu, and Y. P. Sun, EPL **124**, 67005 (2018).
[32]M. Yamaguchi and T. Hashimoto, J. Phys. Soc. Jpn. **32**, 635 (1972).
[33]X.-H. Luo, W.-J. Ren, and Z.-D. Zhang, J. Magn. Magn. Mater. **445**, 37 (2018).
[34]L. H. Bennett and E. D. Torre, J. Appl. Phys. **97**, 10E502 (2005).
[35]C.-K. Tian, C. Wang, W. Ji, J.-C. Wang, T.-L. Xia, L. Wang, J.-J. Liu, H.-X. Zhang, and P. Cheng, Phys. Rev. B **99**, 184428 (2019).
[36]J. Y. Yi, H. L. Zhuang, Q. Zou, Z. M. Wu, G. X. Cao, S. W. Tang, S. A. Calder, P. R. C. Kent, D. Mandrus, and Z. Gai, 2D Mater. **4**, 011005 (2017).